Origin and fate of surface drift in the oceanic convergence zones of the eastern Pacific

C. Maes[1], B. Blanke[1], and E. Martinez[2]

[1]Univ. Brest, Ifremer, CNRS, IRD, Laboratoire d'Océanographie Physique et Spatiale (LOPS), IUEM, F-29280, Brest, France.

[2]IRD, UMR 241 - Écosystèmes insulaires océaniens, Tahiti, French Polynesia.

Corresponding author: Christophe Maes (Christophe.Maes@ird.fr)

Key Points:

- Lagrangian circulation associated with the large-scale surface convergence zones in the eastern Pacific
- Highlighting escape pathways from the center of the convergence zones, with short meridional scales
- Importance of eddy-like variability in structuring the large-scale circulation in a Lagrangian framework

Revised: Friday, March 11, 2016. Accepted.

Abstract

This study investigates the structure and intensity of the surface pathways connecting to and from the central areas of the large-scale convergence regions of the eastern Pacific Ocean. Surface waters are traced with numerical Lagrangian particles transported in the velocity field of three different ocean models with horizontal resolutions that range from ¼° to 1/32°. The connections resulting from the large-scale convergent Ekman dynamics agree qualitatively but are strongly modulated by eddy variability that introduces meridional asymmetry in the amplitude of transport. Lagrangian forward-in-time integrations are used to analyze the fate of particles originating from the central regions of the convergence zones, and highlight specific outflows not yet reported for the Southeastern Pacific when using the currents at the highest resolutions (1/12° and 1/32°). The meridional scales of these outflows are comparable to the characteristic width of the fine-scale striation of mean currents.

1 Introduction

Understanding the long-term variability of the large-scale circulation in the upper ocean remains a challenge despite sustained efforts since the early 1990s. Based on global, direct velocity observations made at the sea surface by drifters (Lumpkin and Johnson 2013) and geostrophic estimates derived both at the surface with altimetric measurements from space, and down to 2000 m depth with the Argo autonomous floats, several studies conclude that the subtropical gyres of the North Pacific and South Pacific have expanded and strengthened since 1993 (see the synthesis given by Rhein et al. 2013). These changes are basically in agreement with the expected dynamical response to observed changes in wind stress forcing, and they are also consistent with the multi-decadal changes in phytoplankton abundances (Martinez et al. 2009a) and sea surface salinity (Chen et al. 2014), especially near the central part of subtropical gyres in the Pacific Ocean.

A knowledge of near-surface currents opens the way toward a variety of other uses, including societal impacts (such as ship routing and rescue efforts), or biological and chemical studies that focus on the transport and dispersion of floating material, whatever their origin and nature. In the Pacific Ocean, which accounts for half of the global ocean area, upper ocean currents and their climate variability largely determine the connectivity of many marine species (e.g., Martinez et al. 2007). The contamination of the marine environment by plastic litter appears as a growing and global problem, with all ocean basins being now contaminated (Eriksen et al. 2014). Though some oceanic regions like the Southern Ocean may still be poorly documented, observed or modeled, surface currents and probabilistic models provide the means for a realistic description of the pathways of marine debris (Potemra 2012; Maximenko et al. 2012; Le Breton et al. 2012, van Sebille et al. 2012). It is worth noting that all of these studies clearly show a surface convergence into five accumulation zones, each of which is associated with the center of a subtropical gyre.

Though the control of these large-scale convergence areas may be related to Ekman currents responding to prevailing anticyclonic winds, Maximenko et al. (2012) noted that the role played by the mesoscale oceanic dynamics is yet to be explored and understood. In their attempt to explain the movement of plastic debris among several islands in the southwestern Pacific, Maes and Blanke (2015) made use of a high horizontal resolution (1/32°) ocean model that explicitly resolved the small-scale dynamics of the upper ocean. They demonstrated that the pathways of the debris can be altered and that their transfer times can be significantly reduced by taking into account the small-scale currents of the upper ocean. In the present study, we use the same methodology and tools to explore the origins and pathways of the surface water masses in the main convergence zones of the Pacific Ocean. The South Pacific convergence zone is of particular interest because it has been shown that the few surface drifters entering this region remain there for the rest of operational lifetime (Martinez et al. 2009b; Maximenko et al. 2012). Our study also points out the need to observe accurate mean currents at high-resolution for a more complete scientific understanding and for the development of applications of benefit to society.

2 Materials and Methods

2.1 Data sets of near-surface ocean currents

We used global velocity datasets from several sources covering the 2007-2010 period: a daily archive of the Naval Research Laboratory (NRL) Layered Ocean Model (hereafter NLOM) analyses at the 1/22.8°×1/32° horizontal resolution (see Shriver et al. 2007; Maes and Blanke 2015); a daily archive of the 1/12° reanalysis of the Hybrid Coordinate Ocean Model (HYCOM) using the Navy Coupled Ocean Data Assimilation (NCODA) system; and a 5-day archive of a NEMO (Nucleus for European Modelling of the Ocean) ocean model experiment run by the DRAKKAR Group (2007) at the ¼° horizontal resolution. For the purposes of the study, the velocity data at the level closest to the surface are extracted only over two areas of interest: the Northeastern Pacific (NP), bounded by 160°W, 120°W, 18°N and 43°N, and the Southeastern Pacific (SP), bounded by 120°W, 80°W, 43°S and 18°S. In the following, we introduce an arbitrary thickness (namely 10 m) to convert all lateral flux estimates into standard transport values. Note that this thickness is not related to the vertical distribution of the layers specific to each model.

2.2 The Lagrangian analysis tool and simulation protocol

The trajectories are simulated with Ariane, a toolkit engineered for the Lagrangian interpretation of the circulation calculated by numerical ocean models (Blanke and Raynaud 1997; Blanke et al. 1999). Since Ariane works on a staggered C-grid, the NLOM and HYCOM velocity components are reprocessed either zonally (for U) or meridionally (for V).

For each model and for each hemisphere, we run two Lagrangian experiments aiming at investigating either the origins or the fates of particles initially distributed over the edges of a small, central rectangular box. The box is 10° wide in longitude and 8° wide in latitude and its center is at 130°W, 30.5°N for the NP, and 100°W, 30.5°S for the SP. The coordinates match the definition of the main subtropical collection areas determined by Maximemko et al. (2012). In the cases of integrations forward in time (i.e., the diagnosis of the fates), the initial particles are distributed over the model grid cells where the transport is outward, for each velocity sample for the year 2007. Conversely, for backward in time integrations, the initial positions are chosen over the cells where the transport is inward, for each velocity sample for the year 2010. The particle trajectories are integrated backward in time until they intercept the outer edges of the domain, or until they recirculate back to the central box, for a maximum time of 3 years that was checked to cover the slowest connection times diagnosed between the central box and the outer limits of the NP and SP domains in the 3 models. The following discussion focuses on the particles that made this traverse.

Vertical movements are not considered, and surface currents are associated with a 10m thick surface layer. Each particle is associated with a fraction of the transport inferred from the local zonal or meridional velocity component (multiplied by the width and thickness of each corresponding grid cell). The sum of all the weights equals the Eulerian outward (inward) transport over the edges of the central box in 2007 (2010). The prescription of a maximum weight equal to 100 m^3/s per particle and per model time record means that 6 to 10 million particles are required for the NLOM and HYCOM currents, and about 20 times fewer than that number for the NEMO currents (due to coarser time sampling and lower energy at small horizontal scales). The volume of water transported from the central box to the outer edges of the domain is computed by summing the transport of the particles that complete the pathway being considered (Döös 1995).

3 Results

By design, the study regions focus on the large-scale upper ocean convergence that characterizes the subtropics in the eastern Pacific. From an Eulerian point of view, the average 2007-2010 net fluxes across the central boxes are always positive, meaning a net convergence. In the SP domain, the values range from 0.07 Sv (NLOM) to 0.67 Sv (HYCOM), while in the NP domain, they range from 0.21 Sv (NEMO) to 0.59 Sv (HYCOM). These values integrated over 4 years represent the subduction of water masses near the center of the gyre (first column of Table 1 – see the supplementary materials). The values obtained for individual years, especially for the initialization years 2007 and 2010, are only a little different, thus indicating a good coherence of the mean transports between the Eulerian and Lagrangian views.

The aggregation of the particle trajectories into a time-integrated transport field shows the most representative pathways that connect the central box and the edge of the domain. The geometry of the transfers is here diagnosed following Blanke et al. (1999), first recording the passage of each particle and summing algebraically its weight at each velocity point of the grid, then deriving a Lagrangian stream function of the resulting non-divergent two-dimensional transport field. The convergence to the central box is shown for both hemispheres on the left part of Figures 1 and 2, for NLOM and HYCOM, respectively. For a given contour interval, the number of contours is directly related to the intensity of the connection under consideration. In the NP, both experiments show the dominance of a source in the mid-latitudes, although the intensity is twice as high in HYCOM as in NLOM (second column of Table 1). In NLOM, there is a direct transfer from the low latitudes, whereas the equivalent connection in HYCOM appears more as an anticyclonic circulation on the scale of the domain with a limited contribution from the western side of the southern frontier. In short, the NLOM experiment suggests the importance of meridional pathways to feed the convergence into the central part of the gyre, in the manner of an integrated Ekman transport, while the HYCOM experiment favors a surface circulation forced by the large-scale wind conditions. For the two models, a similar interpretation can be proposed for the SP. The pathways obtained with NEMO in both hemispheres have certain similarities to HYCOM, but with much less intensity (see figure S1 in the supplementary material). These contrasts reflect the fact that the response of each model to the wind stress is a key element to consider, because it can differ significantly among the 3 configurations as discussed below.

Using the same geometrical configuration in forward integrations lets us investigate the fate of particles originating from each central box, i.e., the central part of each subtropical convergence zone (third column of Table 1 - see the supplementary materials). Our attempts with NEMO could not diagnose any connection to the outer edge of the domains (not shown), meaning that all the particles recirculate toward the central box within 3 years of integration. This result was consistent with the conclusions of the studies discussed earlier that focused on the dynamics of marine debris, in particular in the SP. Interestingly, the Lagrangian integrations made with NLOM and HYCOM show very different behaviors, with the evidence of connections to the remote zonal frontiers (right part of Figures 1 and 2). In both hemispheres, the NLOM velocity field connects mostly the central box to the east of the domain, i.e., the vicinity of the American continent. The intensity of the connection is small in the NP (it amounts to about 6% of the convergence diagnosed in the backward calculations), with a minor secondary southward export. In the SP, the connection is almost exclusively an eastward pathway from the central convergence zone toward the continent, and now amounts to 35% of the remote supply by convergence. For the determination of fates, each connection presents a jet-like structure, with many small-scale patterns that are likely associated with local recirculation.

The results obtained with HYCOM also show a zonal export from the central box in both hemispheres, but with weaker amplitude (13% of the remote supply by convergence in the SP, and only 0.6% in the NP), simpler pathways and smoother structures. It is worth noting that the export is weaker than with NLOM and, in the NP, in the opposite direction (i.e., westward), which likely stems from structural differences in the average currents of the two models (see next section). In the SP, the close agreement obtained between NLOM and HYCOM makes us believe that this region does not behave in fact as a closed region from which floating and drifting marine debris cannot escape. This is not in conflict with the fact that the SP has yet to be identified as an attracting region over long periods (e.g., Froyland et al. 2014), but reveals some pathways for surface floating debris to be expelled from the center of the SP subtropical gyre, a result consistent with the observed longitudinal gradient of litter between the Chilean coast and the Easter Island region (Miranda-Urbina et al. 2015). Our results also stress the fundamental role of eddies and small-scale variability in the context of Lagrangian studies dedicated to the large-scale circulation of the oceans. Noting that the subtropical convergence areas do not behave similarly (i.e., van Sebille et al. 2012), further work is needed to explore the consequences of such variability in the other gyres.

In contrast with the large-scale features associated with the convergence process, the fates of divergent particles show regional patterns with meridional scales of about 200-300 km or less. Thus, outgoing connections are likely more sensitive to the general circulation, large-scale dynamic structures and high horizontal shears that can all modify significantly the dispersion characteristics over the long term. From satellite altimetry, Maximenko et al. (2005) showed time-varying alternating jets (also called striation) in every part of the World Ocean. The strong coupling between these jets and mesoscale eddies both generates new eddies through instabilities and feeds back on the mean ocean currents through rectification. In the northeastern Pacific, Davis et al. (2014) showed that complex processes can also develop from vorticity sources associated with topography and instabilities along the eastern boundary. The average value of the currents in our experiments show such coherent narrow jet-like structures, especially for NLOM (Figure 3, with a color code that highlights the preferred direction of the flow), with an obvious correspondence to the divergent pathways in our analysis and to the presence of a mean eastward flow in both hemispheres. This flow appears in the middle of the central box, on its eastern side (in green in Figs. 1 and 2). This is particularly true in the SP where its zonal extension is longer than 15°, which is enough to connect the central box with the outer edges of the domain.

Though the main directions of the surface flow simulated by HYCOM are similar at the domain scale, the central box is more within a southward and westward flow in the NP. This explains the dominant westward connection obtained when diagnosing the paths of the divergent particles (Fig. 2), whereas NLOM shows a clear eastward connection (Fig. 1). The center of the gyre in HYCOM seems to be offset by about 5° to the northwest compared to NLOM. This suggests that the position of the central box, determined from the annual mean products derived by Maximenko et al. (2012), may not be appropriate for all the models we analyze. This idea is supported by an analysis with the GECKO surface velocity dataset (Sudre et al. 2013), calculated using a different methodology and another wind stress product: it shows that the core of the convergence area in the NP is near 35°N-142°W (figure S2), but it should be noted that the mean currents of this ¼° global product do not show narrow jet-like structures. Yet, sensitivity Lagrangian experiments that were done with HYCOM show that shifting the position of the central box northwestward does not affect the direction and appearance of the outgoing connection. In the SP, the good agreement of the eastward connections toward South America diagnosed in NLOM and HYCOM is explained by equivalent mean eastward currents across the eastern edge of the central box and east of it. Though these tests cannot discriminate precisely between the roles of eddy activity and mean circulation, they call for a better determination of the fine structures of mean currents, which would be valuable to support and confirm the preferential connections diagnosed in a Lagrangian framework.

The structural differences between the mean NLOM and HYCOM mean currents also raise issues about the precise role of mesoscale eddies that are explicitly resolved by NLOM, but not by HYCOM whose resolution is only eddy-permitting. Significantly different Lagrangian results may be expected for coarser and more diffusive models. As already pointed out, it is very difficult to separate the contributions of the mean currents and of eddies because of their entanglement. To partially address this question, we considered the transport of particles with the mean currents of NLOM and found that we could not recover the structure of the diverging pathways revealed by the reference experiment, a result that confirms the crucial role of eddy-like variability for connecting the central regions of the subtropical gyres with the eastern Pacific Ocean (not shown). By contrast, the pathways diagnosed for convergence could be reproduced with some success (see the stream functions in Figure S3), but also with noticeable differences, especially with regard to a reduction in the magnitude of the connections by factors of about 2 and 3 in the NP and SP, respectively (Figure 4). The new results show less scattered pathways and more localized entry points over the edges of the outer domain, with the result that the connection from the eastern Pacific (i.e., from 120°W and 80°W in the NP and SP, respectively) is suppressed. The pathways from the mid-latitudes also changed, with much less central inflow at 43°N and 43°S, which may be a consequence of the removal of the seasonal variability of the surface currents although this point requires further investigation. The suppression of the eddy-like variability also results in convergence with a more or less symmetrical poleward and equatorward pattern in the NP, and symmetry along a southwest-to-northeast axis in the SP.

Thus, from a Lagrangian perspective, the main impact of eddy-like variability is to generate meridional asymmetry on the transport connecting the central convergence zone with the edge of the subtropical gyre (Figure 1). This effect may have important implications for other properties or materials transported by eddies noting that many extratropical eddies are highly nonlinear (i.e., with trapped fluid within the eddy interior) as documented by Chelton et al. (2011).

4 Discussion and conclusions

The Lagrangian analysis of the surface currents from general circulation models provides a convenient interpretation of the convergence and divergence on the scale of subtropical gyres. The explicit consideration of small-scale eddy-like variability is an advance in our understanding of the connections made between the centers of the convergence zones and the edges of the gyres.

In addition to their differences in horizontal resolution, the models differ notably in their number of vertical levels and in the atmospheric forcing that was applied over 2007-2010. NLOM, which was designed to focus on the near-surface, has only 6 dynamical layers plus a mixed layer and its surface wind stress was a hybrid product combining a climatology with operational analyses. HYCOM has 32 vertical hybrid levels (with the shallowest depth of isopycnal layers set at 6 m) and the surface forcing was from the 1-hourly National Centers for Environmental Prediction (NCEP) Climate Forecast System Reanalysis (CFSR). Finally, NEMO used 75 fixed geopotential levels (with the first level set at 0.5 m), and 6-hourly winds and daily heat and freshwater fluxes from the DFS4.1 dataset (Brodeau et al. 2010). The vertical structure of the Ekman spiral and the direction and intensity of the velocity diagnosed near the sea surface will highly depend on the value of the wind stress and on the resolution chosen for the vertical. The way the wind-induced surface circulation of each model will differ accordingly. Despite these differences, the Lagrangian transports as deduced from particle trajectories show quite similar patterns, which suggests that all three models are able to reasonably represent the large-scale convergent Ekman dynamics. We note some modulation of the transports by eddy variability that introduces a poleward/equatorward asymmetry. As noted by Maes and Blanke (2015) in their study of the connections between several archipelagos of the Coral Sea, the eddy mesoscale dynamics explicitly represented by NLOM can influence large-scale transfers as inferred here from diagnosed Lagrangian trajectories.

Contamination of the marine environment by plastic litter is a global issue that will persist for several decades (e.g., Thompson et al. 2009), partly because of the accumulation of such floating debris on the surface of the large-scale zones of convergence in the middle of the subtropical gyres. In the Pacific Ocean, the center of action of these zones is located in the eastern part of the basin where material accumulates over long periods with no apparent means of escape. Our study shows that this last aspect may not be definitive, since escape routes exist in models with sufficient horizontal resolution in which small-scale structures can modify mean currents. Such escape routes are characterized by lateral (mostly meridional) scales of a few hundreds of kilometers, which may explain their omission by previous studies. In the real ocean the trajectory of particles and debris is also affected by physical processes such as surface waves and associated Stokes drift (e.g., Ardhuin et al. 2009) that were not included in our study. More modeling, more observations of currents and analyses that take account of additional geophysical processes (such as windage and waves) are required to understand better the ocean surface currents and, eventually, to develop marine debris collection strategies at the scale of the convergence zones of the subtropical gyres.

Acknowledgments and Data

Our study benefited from different data sets that are freely available on the Internet. This includes the NLOM outputs from APDRC (http://apdrc.soest.hawaii.edu/data/), and the 1/12° global HYCOM+NCODA Ocean Reanalysis was funded by the U.S. Navy and the Modeling and Simulation Coordination Office (output is publicly available at http://hycom.org.GLBu0.08/expt_19.1). The Ariane toolkit is available at http://www.univ-brest.fr/lpo/ariane; We especially thank Dave Berhinger for his patient work on the original manuscript, and the authors would like to acknowledge Erik van Sebille and the other anonymous reviewer for their comments.

References

Ardhuin, F., et al., 2009. Observation and Estimation of Lagrangian, Stokes, and Eulerian Currents Induced by Wind and Waves at the Sea Surface. J. Phys. Oceanogr. 39, 2820-2838.

Blanke, B., Raynaud, S., 1997. Kinematics of the Pacific equatorial undercurrent: An Eulerian and Lagrangian approach from GCM results. J. Phys. Oceanogr. 27, 1038-1053.

Blanke, B., Arhan, M., Madec, G., Roche, S., 1999. Warm water paths in the equatorial Atlantic as diagnosed with a general circulation model. J. Phys. Oceanogr. 29, 2753-2768.

Brodeau, L., B. Barnier, A. M. Treguier, T. Penduff, and S. Gulev, 2010. An ERA40-based atmospheric forcing for global ocean circulation models. Ocean Model., 31, 88–104.

Chelton, D. B., M. G. Schlax, R. M. Samelson, 2011. Global observations of nonlinear mesoscale eddies. Prog. Oceanogr., 91, 167-216, doi:10.1016/j.pocean.2011.01.002.

Chen, J., Zhang R., Wang H., Li J., Hong M., and Li X., 2014. Decadal modes of sea surface salinity and the water cycle in the tropical Pacific Ocean: The anomalous late1990s. Deep-Sea Research I, 84, 38–49.

Davis, A., E. Di Lorenzo, H. Luo, A. Belmadani, N. Maximenko, O. Melnichenko, and N. Schneider, 2014. Mechanisms for the emergence of ocean striations in the North Pacific, Geophys. Res. Lett., 41, 948–953, doi:10.1002/2013GL057956.

Döös, K., 1995. Interocean exchange of water masses in the southern ocean. J. Geophys. Res. 100, 13499-13514.

DRAKKAR Group, 2007. Eddy-permitting ocean circulation hindcasts of past decades. Tech. rep, CLIVAR Exchanges, 12.

Eriksen, M., Lebreton, L.C.M., Carson, H.S., Thiel, M., Moore, C.J., Borerro, J.C., Galgani, F., Ryan, P.G., Reisser, J., 2014. Plastic pollution in the World's oceans: More than 5 trillion plastic pieces weighing over 250,000 tons afloat at sea. PLoS ONE 9(12), e111913. http://dx.doi.org/10.1371/journal.pone.0111913.

Froyland, G., R. M. Stuart, E. van Sebille, 2014. How well-connected is the surface of the global ocean? Chaos, 24, 0331216.

Lebreton LCM, Greer SD., and Borerro JC., 2012. Numerical modelling of floating debris in the world's oceans. Mar. Pollut. Bull. 64, 653–61.

Lumpkin, R., and G. C. Johnson, 2013. Global ocean surface velocities from drifters: Mean, variance, El Niño–Southern Oscillation response, and seasonal cycle, J. Geophys. Res. Oceans, 118, 2992–3006, doi:10.1002/jgrc.20210.

Maes, C., and Blanke B., 2015. Tracking the origins of plastic debris across the Coral Sea: A case study from the Ouvéa Island, New Caledonia. Mar. Pollut. Bull. 97, 160–168.

Martinez, E., Maamaatuaiahutapu, K., Payri, C., and Ganachaud, A., 2007. Turbinaria ornata invasion in the Tuamotu Archipelago, French Polynesia: ocean drift connectivity. Coral Reefs 26 (1).

Martinez, E., D. Antoine, F. D'Ortenzio and B. Gentili, 2009a. Climate-driven basin-scale decadal oscillations of oceanic phytoplankton. Science, 326(5957), 1253-1256.

Martinez, E., Maamaatuaiahutapu, K., and Taillandier, V., 2009b. Floating marine debris surface drift: convergence and accumulation toward the South Pacific subtropical gyre. Mar. Pollut. Bull. 58, 1347–1355.

Maximenko, N. A., B. Bang, and H. Sasaki (2005), Observational evidence of alternating zonal jets in the world ocean, Geophys. Res. Lett., 32, L12607, doi:10.1029/2005GL022728.

Maximenko, N.A., Hafner J. and Niiler P.P., 2012. Pathways of marine debris derived from trajectories of Lagrangian drifters Mar. Pollut. Bull. 65 51–62.

Miranda-Urbina, D., M. Thiel, G. Luna-Jorquera, 2015. Litter and seabirds found across a longitudinal gradient in the South Pacific Ocean. Mar. Pollut. Bull. 96, 235–244.

Potemra, J. T., 2012. Numerical modeling with application to tracking marine debris. Mar. Pollut. Bull. 65, 42–50.

Rhein, M., S.R. Rintoul, S. Aoki, E. Campos, D. Chambers, R.A. Feely, S. Gulev, G.C. Johnson, S.A. Josey, A. Kostianoy, C. Mauritzen, D. Roemmich, L.D. Talley and F. Wang, 2013. Observations: Ocean. In: Climate Change 2013: The Physical Science Basis. Contribution of Working Group I to the Fifth Assessment Report of the Intergovernmental Panel on Climate Change [Stocker, T.F., D. Qin, G.-K. Plattner, M. Tignor, S.K. Allen, J. Boschung, A. Nauels, Y. Xia, V. Bex and P.M. Midgley (eds.)]. Cambridge University Press, Cambridge, United Kingdom and New York, NY, USA.

Shriver, J.F., Hurlburt, H.E., Smedstad, O.M., Wallcraft, A.J., and Rhodes, R.C., 2007. 1/32° real-time global ocean prediction and value-added over 1/16° resolution. J. Mar. Syst. 65, 3–26.

Sudre J., Maes C., and Garcon V., 2013. On the global estimates of geostrophic and Ekman surface currents. Limnol. Oceanogr.: Fluids Environ. 3, 1–20. http://dx.doi.org/10.1215/21573689-2071927.

Thompson, R.C., Moore, C.J., vom Saal, F.S., Swan, S.H., 2009. Plastics, the environment and human health: current consensus and future trends. Philosophical Transactions of the Royal Society of London B: Biological Science 364 (1526), 2153e2166.

van Sebille E., England M.H. and Froyland G., 2012. Origin, dynamics and evolution of ocean garbage patches from observed surface drifters. Environ. Res. Lett. 7, 044040.

Figure 1.

NLOM Lagrangian stream function for the surface volume transfer between the central box (purple) and the edge of the outer domain (green, red, yellow and blue sections) in the northeastern Pacific (top) and southeastern Pacific (bottom). The contour interval is 0.01 Sv, except for the outgoing connection diagnosed in the NP (0.001 Sv to highlight the jet-like structure). Left: origins of the converging flow considered in 2010 across the central box. Right: Fates of the diverging flow considered in 2007 across the central box.

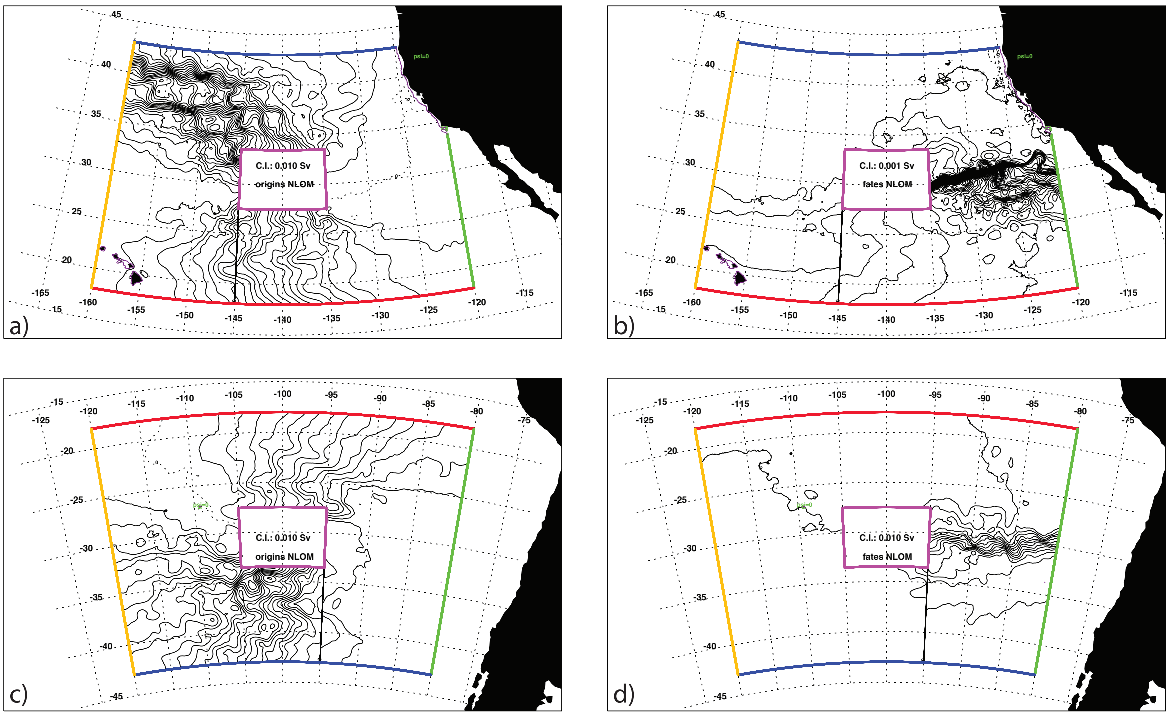

Figure 2. Same as Figure 1 but for HYCOM

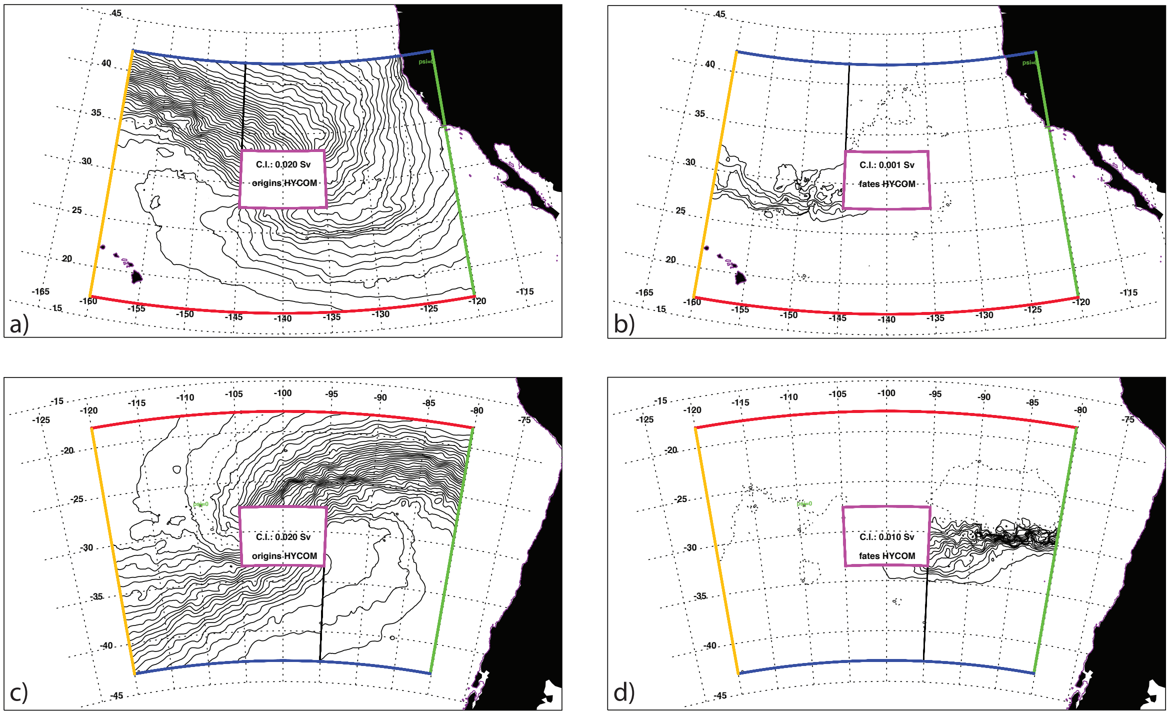

Figure 3

Mean annual surface currents (2007-2010) for NLOM (left) and HYCOM (right), and for the northeastern Pacific (top) and southeastern Pacific (bottom), shown as vectors extrapolated on a ¼° grid over the domain of the Lagrangian integrations. The color code refers to the dominant direction of the flow: mostly poleward (blue), westward (orange), equatorward (red), eastward (green).

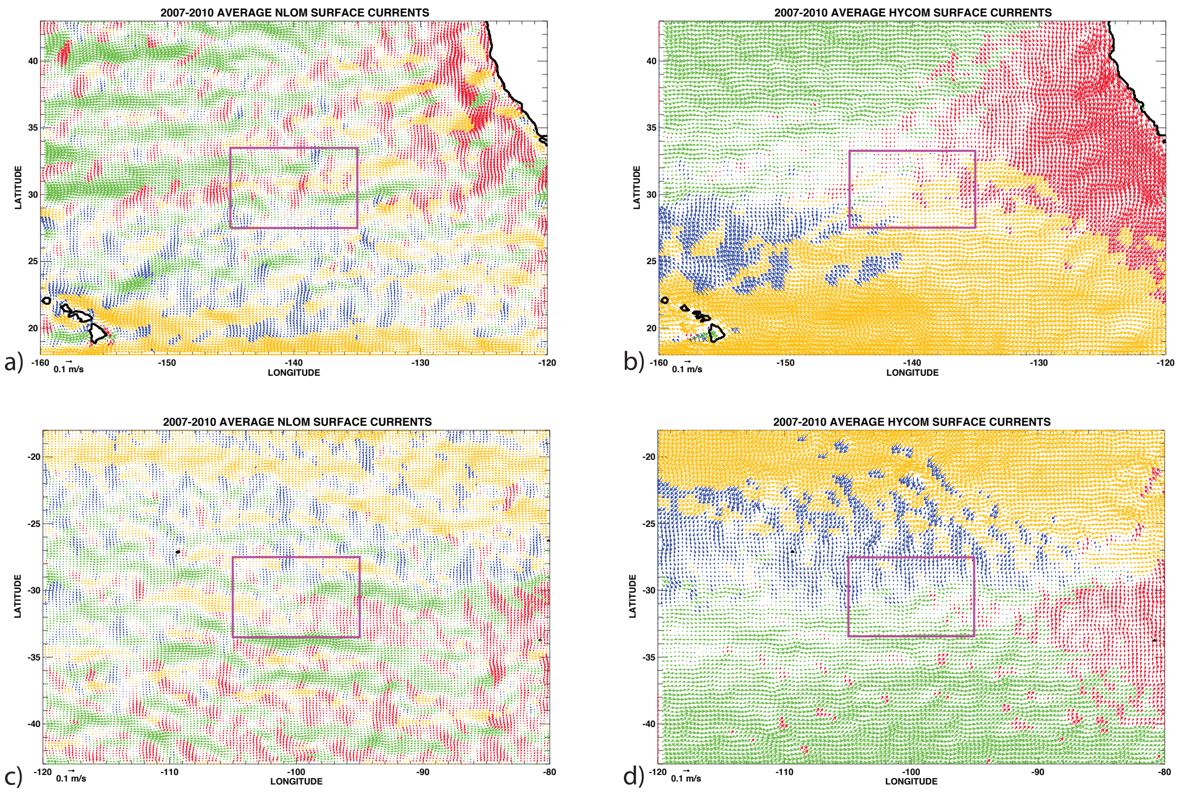

Figure 4

Cumulative transport (in Sv) transferred from the central box, starting integration from 43°N 160°W (Top: NP) or 43°S 120W (Bottom: SP). The result is colored according to the edge of the outer domain where the interception is made (see Figure 1) and is shown both for the Lagrangian integration using the daily (thick line) and mean (dotted line) NLOM currents.